Signatures of two-dimensional superconductivity emerging within a three-dimensional host superconductor

Carolina Parra[a,b,c,d,1], Francis C. Niestemski[a,b,c], Alex W. Contryman[a,c,e], Paula Giraldo-Gallo[f], Theodore H. Geballe[c,e], Ian R. Fisher[a,c,e], and Hari C. Manoharan[a,b,c,1]

[a]SLAC National Accelerator Laboratory, Stanford Institute for Materials and Energy Sciences, Menlo Park, CA 94025; [b]Department of Physics, Stanford University, Stanford, CA 94305; [c]Geballe Laboratory for Advanced Materials, Stanford University, Stanford, CA 94305; [d]Laboratorio de Nanobiomateriales, Departamento de Física, Universidad Técnica Federico Santa María, Valparaíso 2390123, Chile; [e]Department of Applied Physics, Stanford University, Stanford, CA 94305; and [f]Department of Physics, Universidad de Los Andes, Bogotá 111711, Colombia

Edited by Zachary Fisk, University of California, Irvine, CA, and approved February 22, 2021 (received for review August 21, 2020)

Spatial disorder has been shown to drive two-dimensional (2D) superconductors to an insulating phase through a superconductor–insulator transition (SIT). Numerical calculations predict that with increasing disorder, emergent electronic granularity is expected in these materials—a phenomenon where superconducting (SC) domains on the scale of the material's coherence length are embedded in an insulating matrix and coherently coupled by Josephson tunneling. Here, we present spatially resolved scanning tunneling spectroscopy (STS) measurements of the three-dimensional (3D) superconductor $BaPb_{1-x}Bi_xO_3$ (BPBO), which surprisingly demonstrate three key signatures of emergent electronic granularity, having only been previously conjectured and observed in 2D thin-film systems. These signatures include the observation of emergent SC domains on the scale of the coherence length, finite energy gap over all space, and strong enhancement of spatial anticorrelation between pairing amplitude and gap magnitude as the SIT is approached. These observations are suggestive of 2D SC behavior embedded within a conventional 3D *s*-wave host, an intriguing but still unexplained interdimensional phenomenon, which has been hinted at by previous experiments in which critical scaling exponents in the vicinity of a putative 3D quantum phase transition are consistent only with dimensionality $d = 2$.

superconductivity | superconductor–insulator transition | phase transitions | reduced dimensions | scanning tunneling microscopy and spectroscopy

In the two-dimensional (2D) limit of the superconductor–insulator transition (SIT) (1–3), there is evidence of emergent electronic granularity in numerical simulations (4–6) and thin-film experiments (7–10). It has been recently discovered (11, 12) that bulk three-dimensional (3D) $BaPb_{1-x}Bi_xO_3$ (BPBO) (Fig. 1*A*) exhibits a magnetic field–tuned SIT with unexpected 2D scaling which hints at a "hidden" two dimensionality in the superconductivity. Lacking further experiments, the origin of this interdimensional order was not clear. For example, the phase could be emergent due to increased interactions and localization near the SIT. Such unusual scaling behavior has also been connected to a partially disordered stripe-like nanoscale structural phase separation due to the fact that the stripe width matches the superconducting coherence length at the Bi composition which maximizes T_c (the optimal doping point) (13, 14). Additionally, the role played by the high-temperature dimorphic nature of BPBO (two coexisting crystal structures with different electronic properties) in the composition range $x = [0.18–0.30]$ (Fig. 1*B*) on the low-temperature electronic structure is not known. This possible competition between emergence, macroscopic electronic properties, and microscopic structure is fascinating, but a detailed study of the local electronic superconducting and localization properties and their connection to disorder potential was necessary to provide further insight.

Scanning tunneling microscopy and spectroscopy (STM/STS) enable a local probe of the electronic properties through measurements of local density of states (LDOS) along with topographic information. This technique has been used to study the LDOS homegeneity in quasi-2D superconductors (SC), including high-T_c superconductors (HTSC) (15–17) and 2D thin-film SC systems (10, 18–20). STS reports that examine the influence of disorder on the SC state in 3D systems are limited (21, 22).

Motivated by these challenges, we performed topographic and spatially resolved LDOS measurements of BPBO for three Bi compositions, $x = 0.19$, 0.25, and 0.28, which we refer to as x_{low}, x_{opt}, and x_{high}, respectively. All measurements were performed at 4.4 K, well below T_c for all dopings measured; hence, we are exploring the component of the phase diagram consisting of the superconducting dome as we approach the SIT from under-doping through optimal doping to over-doping (Fig. 1*A*). Our results are summarized in Fig. 1*C*, which show spatially resolved properties for $x = 0.28$, the Bi composition closest to the SIT. The electronic properties extracted from LDOS measurements (coherence peak height h_{cp} and gap size

Significance

We report signatures of a new phenomenon wherein a hidden "interdimensional" order emerges from a bulk three-dimensional superconductor tuned to approach a phase transition to an insulator. Prior electrical transport measurements found that the superconductor–insulator transition of $BaPb_{1-x}Bi_xO_3$ demonstrated critical scaling behavior but inexplicably required parameters consistent only with two dimensions. Here, we directly image the three-dimensional superconducting state as it approaches an insulating phase and discover that signatures of a two-dimensional granular superconducting phase spontaneously emerge at the transition. Moreover, the properties of this phase precisely match the theory of emergent electronic granularity specific to two-dimensional materials. These findings posit that a three-dimensional superconductor electronically reorganizes itself into a two-dimensional granular superconductor before ultimately transforming to an insulator.

Author contributions: C.P., A.W.C., and H.C.M. designed research; C.P., A.W.C., and P.G.-G. performed research; T.H.G., I.R.F., and H.C.M. contributed new reagents/analytic tools; C.P., F.C.N., A.W.C., P.G.-G., T.H.G., I.R.F., and H.C.M. analyzed data; C.P., A.W.C., P.G.-G., and H.C.M. wrote the paper; and H.C.M. directed the project.

The authors declare no competing interest.

This article is a PNAS Direct Submission.

[1]To whom correspondence may be addressed. Email: carolina.parra@usm.cl or manoharan@stanford.edu.

This article contains supporting information online at https://www.pnas.org/lookup/suppl/doi:10.1073/pnas.2017810118/-/DCSupplemental.

Published April 12, 2021.

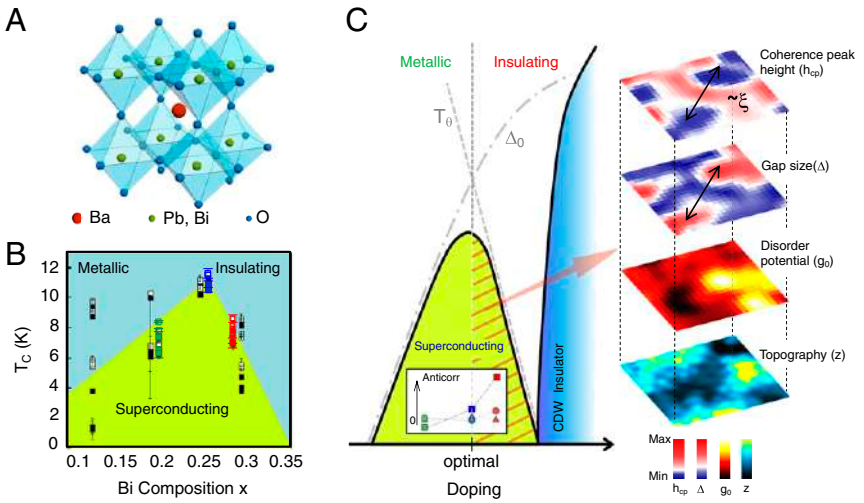

Fig. 1. BPBO structure and electronic phase diagram. (*A*) Perovskite-like crystalline structure of three-dimensional BPBO single crystal. Orthorhombic and tetragonal phases result from rotational instabilities of the O_6 units. (*B*) Electronic phase diagram of BPBO as a function of temperature and Bi composition (x), exhibiting a superconducting dome peaked at $x = 0.25$ (optimal doping). Critical temperature (T_c) values were obtained from measurements of resistivity (full and open squares) and magnetic susceptibility (full circles) (11). Compositions studied in this work are highlighted in green ($x = 0.19$), blue ($x = 0.25$), and red ($x = 0.28$). (*C*) Diagram summarizing coherence peak height (h_{cp}, a measure of SC pairing amplitude), energy gap size (Δ), zero-bias conductance (g_0, a measure of disorder potential), and topography (z, a measure of physical disorder) from our spatially resolved observations for BPBO near the SIT ($x = 0.28$). The inset shows anticorrelation between measured features as a function of Bi composition. Anticorrelation between Δ and h_{cp} (squares) increases near the SIT, while anticorrelation between Δ and g_0 (circles) and between h_{cp} and g_0 (triangles) remain low.

Δ) show a distinct spatial anticorrelation and have a characteristic length scale ξ, which we show is very close to the calculated BPBO coherence length. These properties are uncorrelated with measurements of disorder potential g_0 and topography z. These observations are all consistent with an emergent electronic granularity at $x = 0.28$. The spatial correlations between properties for all Bi compositions are summarized in the anticorrelation plot in Fig. 1*C*.

dI/*dV* measured along a line for the three Bi compositions is shown in Fig. 2, providing an overview of the inhomogeneity analyzed in the rest of the paper. The spectra contain SC gaps of varying type, ranging from those with strong coherence peaks (yellow) to those with muted coherence peaks (red). The gap size Δ, defined as half the peak-to-peak distance, is measured utilizing derivative analysis to determine maxima. For optimally doped samples (Fig. 2*B*), the spectra are mostly symmetric with strong coherence peaks. In contrast, spectra measured for samples away from x_{opt} tend to be asymmetric with coherence peaks less well defined (Fig. 2 *A* and *C*). The gap size and coherence

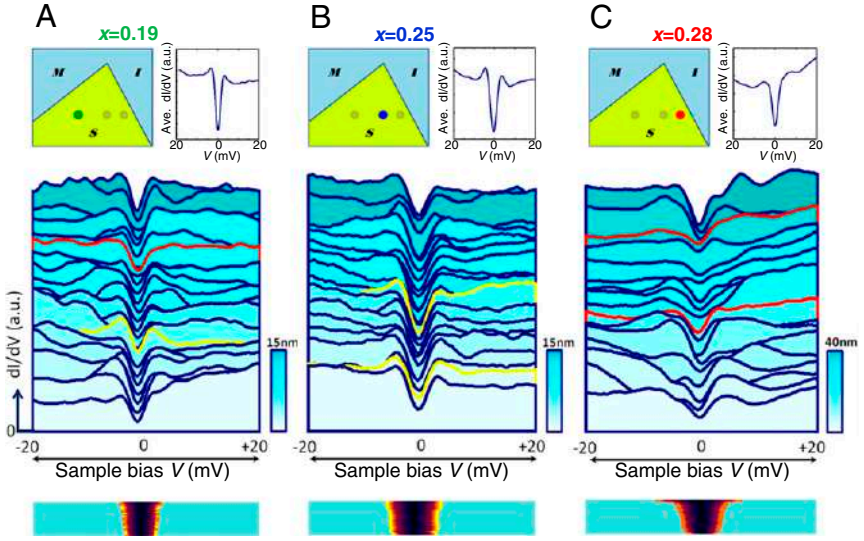

Fig. 2. Spatial variation snapshots of the local density of states. Measurements of *dI*/*dV* along a line of length 15 nm for $x = 0.19$ (*A*), $x = 0.25$ (*B*), and 40 nm for $x = 0.28$ (*C*) ($I = 200$ pA). Upper insets show corresponding position in the x–T_c phase diagram and the spatially-averaged *dI*/*dV* curve. STS spectra show symmetric gap with (yellow spectra) and without (red spectra) coherence peaks at the gap edge. Each lower color snapshot plots all *dI*/*dV* spectra acquired along the line, but here spectra are stacked up along the vertical axis and arranged by increasing gap magnitude. For each snapshot, the horizontal axis matches the sample bias scale for the corresponding linecut (*A*–*C*), and *dI*/*dV* magnitude is represented by a color scale ranging from black through orange up to yellow (regions outside the gap are identified in light blue). In this visualization, gap edges with strong coherence peaks are highlighted in yellow, gap edges with weak coherence peaks appear orange, and the gap region appears in dark colors.

peaks are strongly inhomogeneous for x_{high}. These spatial variations in the magnitude of Δ have been explored before in STS studies of HTSCs (15, 23, 24) and SC thin films (8–10, 18–20, 25) but thus far not reported in a conventional 3D SC system.

The gap (Δ) and normalized coherence peak height ($\tilde{h}_{cp}$) variations are quantified by the histograms plotted in Fig. 3 *A* and *B*. The coherence peak height h_{cp} is determined by measuring the average of the coherence peak height at positive and negative bias relative to a curve passing through the high bias background (see Fig. 5*A* for schematic). That value is then normalized by the highest h_{cp} value to determine $\tilde{h}_{cp}$. The most frequent Δ and $\tilde{h}_{cp}$ values were found by fitting the histograms to Gaussians and are shown with corresponding bars depicting the SDs in Fig. 3 *C* and *D*, respectively. Here we observe that both Δ and $\tilde{h}_{cp}$ as a function of Bi composition follow a trend similar to the dome-like behavior of the critical temperature T_c (see inset between Fig. 3 *C* and *D*). This is in stark contrast to other SC systems such as hole-doped cuprates where measured gap with doping does not appear to follow T_c (15). Since the coherence peaks are directly associated with the phase coherence in the superconductor (5, 6, 8, 26), the height of the coherence peaks provides a direct measure of the local SC order parameter phase stiffness. The obtained $\tilde{h}_{cp}$ dome-like behavior (Fig. 3*D*) confirms an increase of SC disorder in BPBO (loss of global superconductivity) for Bi compositions away from x_{opt}.

According to the observed spatial gap variation, which is widely understood as a measure of SC disorder (25, 27–29), SC disorder in BPBO increases considerably for samples with Bi composition away from x_{opt}. From x_{opt} to x_{high}, variations in gap size range from 35 to 243%. At x_{high}, there is an important asymmetry in the variation of Δ (red histogram in Fig. 3*A*), weighted toward higher values. Observed asymmetry in Δ variations for x_{high} suggests that disorder displaces Δ toward higher values (instead of toward lower values as a SC dome would indicate). This leads to a SC phase half-dome shape similar to the one observed for $Ba_{1-x}K_xBiO_3$ (30–33).

The normalized SC gap, $2\Delta/k_BT_c$, where k_B is the Boltzmann constant, is the best indicator of the electron–phonon coupling strength within mean field theory (34). For a superconductor with strong coupling, $2\Delta/k_BT_c$ is larger than the value expected for BCS theory in the weak coupling limit, 3.52 (35). The value of the electron–phonon coupling strength for each doping, according to our tunneling spectroscopy data combined with critical temperatures obtained from resistivity and magnetic susceptibility measurements (Fig. 1*B*), is $2\Delta/k_BT_c \sim 9$, 9.7, and 11.6 for $x = 0.19$, 0.25, and 0.28, respectively. This trend might be due to a progressive increase in electron–phonon coupling strength as function of Bi composition. A similar increase has been seen in BPBO using macroscopic point-contact tunneling measurements (36, 37). However, those reports showed a $2\Delta/k_BT_c$ value of 2.3 for $x = 0.18$ that saturates to the BCS value above $x = 0.22$.

These results can be understood in terms of disorder. For strongly disordered superconductors, Δ is expected to be much larger than the pairing field which leads (when moving toward the SIT) to a lower macroscopic T_c value that is no longer determined by Δ (19). For BPBO samples near the SIT, macroscopic T_c values (11, 36, 38, 39) would be then suppressed due to phase incoherence effects originated in the spatial disorder. Hence controlling disorder would be a key to increasing T_c in this material, which in turn would decrease the $2\Delta/k_BT_c$ ratio, approaching the BCS estimate. Similar interpretation of an anomalously large $2\Delta/k_BT_c$ has been explored in NbN (8) and InO (19) thin films.

To visualize spatial variations, we map the SC gap values for the three Bi compositions over nanometer-scale areas (Fig. 4). The color bar below each map shows the range of Δ measured for that particular composition, which varies from 1.1 to 12 mV across all compositions. Percentage variation with respect to the mean gap value as previously seen in Fig. 3*A* is represented by the right color scale bar. Large spatial variations of Δ were found

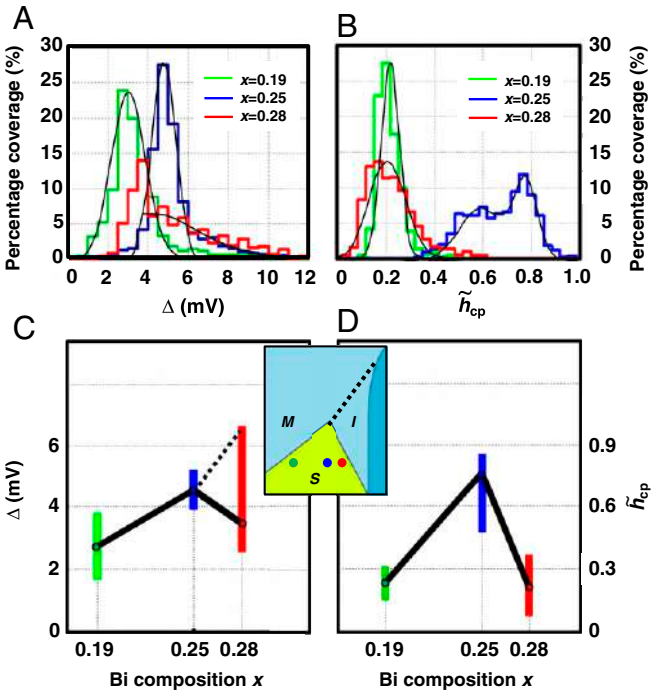

Fig. 3. Statistics of the gap size and coherence peak inhomogeneity. (*A* and *B*) Histograms of Δ and h_{cp} respectively obtained from STS for samples with $x = 0.19$, 0.25, and 0.28. A Gaussian has been fit to each histogram to quantify the mean gap value and the gap variation. Since Δ for $x = 0.28$ and $h_{cp}$for $x = 0.25$ are so asymmetric, two separate Gaussians were fit for each side of the data (only one shown in the case of gap). Values of h_{cp} were normalized to the highest measured value. (*C* and *D*) Gap size and coherence peak height as a function of Bi concentration obtained from histogram in *A* and *B*, with corresponding bars denoting SD. Δ and $\tilde{h}_{cp}$ values versus *x* follow a dome-like shape matching the *x*-versus-T_c phase diagram (inset). However, strong asymmetry for Δ variations for $x = 0.28$ is observed (red bar), biased toward higher gap values (dashed black line).

for x_{high} (Fig. 4*C*), in contrast to the more homogeneous gap values measured for x_{opt} doping (Fig. 4*B*). The characteristic length scale of the gap inhomogeneity for $x = 0.28$ is measured to be 4.5 ± 0.5 nm according to spatial correlation analysis. This is comparable to the Ginzburg–Landau coherence length ξ (~5 nm, obtained from upper critical field $H_{c2}(T)$ measurements through the standard Werthamer–Helfand–Hohenberg approximation) for the same doping, in addition to being similar to the length scale of structural phase separation, ~8 nm (11, 13).

The observed spatial inhomogeneity in the SC gap is unrelated to topographic disorder as measured by STM. Due to the 3D nature of the crystal, topographic images show a highly disordered surface for all Bi compositions (*SI Appendix*, Fig. S1) with characteristic length scales ranging from atomic level up to ~3 nm. For x_{high}, both the topography (*z*) and zero-bias conductance (g_0) map are uncorrelated with the observed SC electronic disorder (*SI Appendix*, Fig. S2).

Recent zero-field-cooled magnetic susceptibility measurements of the SC volume fraction (12) show a maximum value of 45% for $x = 0.25$, which was attributed to structural dimorphism. A higher SC volume fraction of around 70% was measured in a different study (40). Our local measurements show that even though the local gap size is highly inhomogeneous for Bi compositions close to the SIT, there exists a finite gap over all space.

It was previously mentioned that Δ and $\tilde{h}_{cp}$ values follow the same dome-like behavior of T_c with varying Bi composition, but we now seek further information connecting these two parameters from a spatially resolved point of view. This analysis uncovers a

PHYSICS

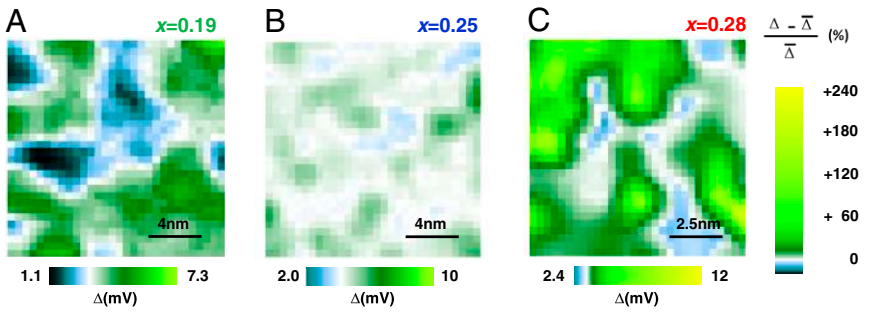

Fig. 4. Spatial gap inhomogeneity in the superconducting dome. Map of spatial variations of the SC gap of BPBO, deduced from STS experiments for different Bi concentrations: *A*, x_{low} (15×15 nm^2), *B*, x_{opt} (15×15 nm^2), and *C*, x_{high} (9×9 nm^2) ($I = 100$ to 200 pA). Overall gap size variations range from 1.6 to 6.6 mV. Corresponding gap values are represented by the color scale bar below each map. The right color scale bar is defined as percentage variation of gap size with respect to the mean gap value (0% or white). Areas with colors ranging from green to yellow correspond to points where gap size exceeds the mean Δ value, while colors ranging from light to dark blue are associated with gaps below the mean Δ value.

striking behavior: Δ and $\tilde{h}_{cp}$ become strongly spatially anticorrelated for Bi compositions near the SIT (Fig. 5). Comparing three representative *dI*/*dV* spectra (Fig. 5*A*, acquired from positions marked α, β, and γ in Fig. 5*B* from an x_{high} sample), strong variations in h_{cp} and in Δ can be seen. In fact, the magnitudes of these two values are visibly anticorrelated. To highlight this anticorrelation, Δ and $\tilde{h}_{cp}$ maps for $x = 0.28$ are plotted in Fig. 5 *B* and *C*. The anticorrelation for x_{high} is quantified in a two-parameter histogram (Fig. 5*D*) that shows a count distribution with negative slope and a cross-correlation value of $r = -0.42$, indicating a robust anticorrelation. In contrast, very weak correlation coefficients are found for $x = 0.19$ and $x = 0.25$, with $r = +0.1$ and $r = -0.14$, respectively (See *SI Appendix*, Fig. S3 for all maps). In addition, zero-bias conductance measurements, a measure of potential disorder (41), show an even weaker correlation with Δ and $\tilde{h}_{cp}$ ($r = -0.1$ and $r = 0.01$, respectively) (*SI Appendix*, Figs. S3 and S4).

The signatures presented here suggest that an emergent electronic granularity is present in BPBO at x_{high}. This has been theoretically predicted to occur in 2D superconductors (4–6, 42) and experimentally observed in 2D systems, such as InO (7, 19), NbN (8, 25, 43), and TiN (2, 18) thin films, where temperature is the parameter used to tune disorder in analogy to how Bi composition acts in our system. In this picture, SC domains in BPBO close to the SIT, which are separated by insulating areas with size comparable to the coherence length, become correlated through coherent Josephson tunneling of Cooper pairs between the SC domains. This would lead to the apparent absence of insulating domains in our local spectroscopic measurements. One possible interpretation of SC gap and coherence peak height maps for $x = 0.28$ is that areas with wider gap values and smaller coherence peak height (red areas in Fig. 5*B* and blue areas in Fig. 5*C*) can be associated with insulating domains (which show a gap due to proximity effects) that are separated by SC domains (smaller gap values and larger coherence peak height in Fig. 5 *B* and *C*), although the one-to-one identification might not be as simple as suggested by the anticorrelation relation between gap size and coherence peak height. The $\tilde{h}_{cp}$ map (Fig. 5*C*) shows a granular structure with a characteristic length scale of 4.4 ± 0.5 nm, in close agreement with the length scale for the Δ spectral map quoted above. Both of these length scales are comparable to the calculated coherence length, a feature shared by systems with emergent electronic granularity (44). Additionally, our observation of a finite gap over all space supports this picture. Finally, the anticorrelation between gap size and coherence peak height (associated with pairing amplitude) that occurs most strongly at $x = 0.28$ provides a third signature of emergent electronic granularity.

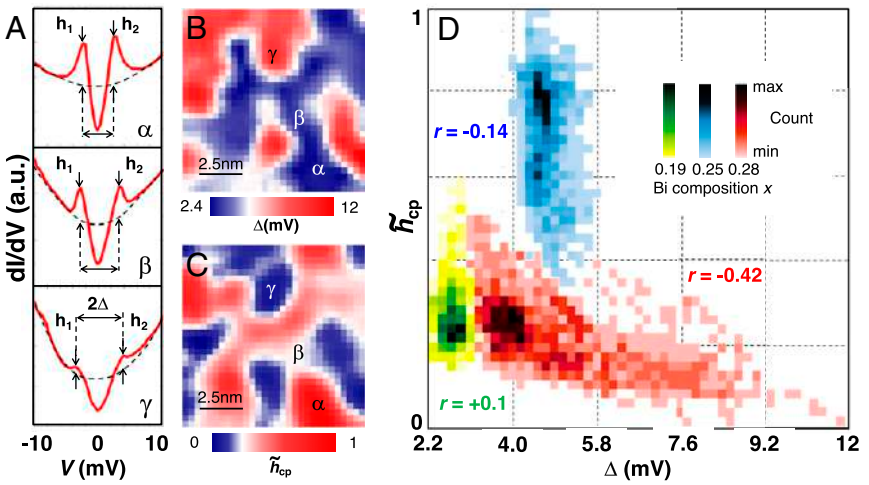

Fig. 5. Correlation between superconducting gap and pairing amplitude. (*A*) Representative spectra taken at points α, β, and γ in *B* (or *C* equivalently). Spatial variation of SC gap (*B*) and coherence peak height (*C*) for Bi composition $x = 0.28$ (9×9 nm^2). An anticorrelation between Δ and $\tilde{h}_{cp}$ is clearly observed for this Bi composition closest to the SIT. (*D*) Two-parameter histogram of Δ and $\tilde{h}_{cp}$ for $x = 0.19$ (green color scale), $x = 0.25$ (blue color scale) and $x = 0.28$ (red color scale). Cross-correlation values *r* for each composition are displayed in green (+0.1), blue (−0.14), and red (−0.42).

We contextualize this interpretation within the framework of other intertwined orders such as a relationship between the superconductivity and structural polymorphism [studied previously using high resolution TEM (13)] and a proximal charge density wave (CDW) phase. The similarity between electronic length scales, coherence length, and structural polymorph segregation length scale (13) is enigmatic. However, no strong correlation between the gap size and the two measures of spatial disorder (topography z, potential disorder g_0) are observed (*SI Appendix*, Figs. S3 and S4), suggesting that the electronic length scales are emergent. Notably, the structural polymorphs are not identified via STM topography, although the crystal is viewed through the disordered surface. Interestingly, our BPBO samples are in close proximity to a competing CDW phase. Such a CDW phase—if coexistent with superconductivity—would manifest itself with an energy gap, which creates a possible ambiguity in our data: Are the gaps (especially those with small coherence peaks) due to superconductivity or a charge density wave phase? Evidence favors the superconductivity interpretation. First, CDW order has only been observed in the normal state and not simultaneously in the superconducting state, although coexistence was conjectured due to overlapping crystal dopings (45). However, and most significantly, typical CDW gaps in bismuthates are almost an order of magnitude larger than the gaps observed in this work (45–47).

Although BPBO is expected to be an *s*-wave superconductor, it apparently shares some phenomenology of *d*-wave layered superconductors such as anticorrelation between Δ and h_{cp} and the "V"-shape of dI/dV spectra seen in Figs. 5*A* and 2 (typical of underdoped cuprates) (48). This *d*-wave resemblance has been discussed before for *s*-wave SC films (4) in terms of gap persistence across phase transitions. However, the role of disorder over this phenomenology, mainly driven by the proximity to a Mott insulator, is expected to be secondary. Additionally, our data show how the pairing amplitude h_{cp} for $x = 0.28$ covers a very wide range of values including being completely suppressed for the largest gap values, in contrast to previously reported data from cuprates (48) where such behavior is not as extreme. Gap variations are also extreme at $x = 0.28$, significantly larger than the reported values for cuprates (15).

In conclusion we found in BPBO—a bulk 3D SC material—three signatures expected for 2D SC systems near a SIT: evidence for an emergent electronic granularity on the scale of the SC coherence length ξ, finite energy gap over all space, and strong spatial anticorrelation between energy gap Δ and pairing amplitude h_{cp}. The length scale of electronic disorder is uncorrelated with local structural disorder as measured by STM, supporting the emergent nature of the observed granularity. Our observations suggest a complex interplay between the low-temperature superconductivity, the electronic disorder landscape, high-temperature microstructure, and localization.

The observed crossover in length scales for electronic granularity and ξ could possibly explain the previously reported but unexplained 2D critical scaling at a quantum phase transition in BPBO. There has been recent work in one-dimensional (1D) disordered superconducting nanowires showing that 2D scaling anomalously provides superior "scaling collapse," which may point to a reverse microscopic phenomenon (49). On the other hand, it was explicitly noted that for BPBO, the scaling data for all of the compositions studied could not be fit to a 3D quantum phase transition and ruled out any temperature-dependent prefactor $T^{-(d-2)/z}$ in the resistivity; hence, $d = 2$ provided the best scaling for more than three orders of magnitude in the scaling variable (11). We note that recent theoretical studies of duality between superconducting and superinsulating phases enable a 3D generalization of 2D emergent granularity (50, 51).

Local pairing amplitude measurements for x_{high} samples are larger than expected based on the macroscopic T_c values, which implies that this material has a higher intrinsic T_c that is limited by disorder. Statistical analysis of spatially resolved measurements suggests that the SIT is determined by phase rather than amplitude fluctuations. Our results also raise the question of whether the origin of V-shape conductance spectra is due to *d*-wave pairing as in the case of cuprates, or simply due to electronic disorder. Notably, the 3D superinsulator phase has been conjectured to be associated with the pseudogap phase of high-temperature superconductors (52). Very recently, numerical calculations have suggested that a disordered superconductor driven through the 3D Anderson transition shares some of the 2D phenomenology, including strong spatial fluctuations and enhancements of the order parameter, although only in the weak-coupling limit, and specific connections to local variables accessible via STM/STS are out of reach (53). Our work presents a detailed study of local effects of disorder in a 3D SC system, and we expect that it will be a first step in understanding the interdimensional interconnection in local SC behavior between 2D and 3D quantum materials.

Methods

Single crystals of BPBO with $0.19 < x < 0.28$ were grown using a self-flux technique similar to the one described in (11). The Bi composition was determined by electron microprobe analysis. These measurements revealed a uniform composition across each sample within an experimental uncertainty of ± 0.02 in x.

The spatial variations of spectral features were measured by performing STM/STS measurements on BPBO with three different Bi compositions: $x = 0.19$ (under doped), $x = 0.25$ (optimally doped), and $x = 0.28$ (over doped). The sample was mechanically cleaved in ultrahigh vacuum (UHV) at 77 K and then immediately placed into a cryogenic STM held at 4.4 K. We obtained STM topographs in constant-current mode using a chemically etched tungsten tip that was first verified on a Au(111) surface for sharpness, cleanliness, and spectral flatness. The differential conductance dI/dV was measured by using a standard lock-in technique with sinusoidal bias modulation of 100 μV to 1 mV and a frequency of 757 Hz. Typical junction resistances were between 1.5 and 3 MΩ.

Data Availability. All study data are included in the article and/or *SI Appendix*.

ACKNOWLEDGMENTS. This work was supported by the US Department of Energy, Office of Science, Basic Energy Sciences, Materials Sciences and Engineering Division, under Contract DE-AC02-76SF00515. C.P. acknowledges Agencia Nacional de Investigación y Desarrollo, Programa de Investigación Asociativa, Grant ANID PIA Anillo ACT192023, Fondecyt 1191353, and Fondecyt 1180702. We thank S. Kivelson, M. Beasley, and D. Shahar for discussions.

1. A. M. Goldman, N. Markovic, Superconductor-insulator transitions in the two-dimensional limit. *Phys. Today* **51**, 39–44 (1998).
2. T. I. Baturina, A. Y. Mironov, V. M. Vinokur, M. R. Baklanov, C. Strunk, Localized superconductivity in the quantum-critical region of the disorder-driven superconductor-insulator transition in TiN thin films. *Phys. Rev. Lett.* **99**, 257003 (2007).
3. A. T. Bollinger *et al.*, Superconductor-insulator transition in $La_{2-x}Sr_xCuO_4$ at the pair quantum resistance. *Nature* **472**, 458–460 (2011).
4. K. Bouadim, Y. L. Loh, M. Randeria, N. Trivedi, Single- and two-particle energy gaps across the disorder-driven superconductor-insulator transition. *Nat. Phys.* **7**, 884–889 (2011).
5. N. Trivedi, Y. L. Loh, K. Bouadim, M. Randeria, Emergent granularity and pseudogap near the superconductor-insulator transition. *J. Phys. Conf. Ser.* **376**, 012001 (2012).
6. N. Trivedi, Y. L. Loh, K. Bouadim, M. Randeria, Aspects of localization across the 2D superconductor-insulator transition. *Int. J. Mod. Phys. Conf. Ser.* **11**, 22 (2012).
7. D. Kowal, Z. Ovadyahu, Disorder induced granularity in an amorphous superconductor. *Solid State Commun.* **90**, 783–786 (1994).
8. A. Kamlapure *et al.*, Emergence of nanoscale inhomogeneity in the superconducting state of a homogeneously disordered conventional superconductor. *Sci. Rep.* **3**, 2979 (2013).
9. C. Carbillet *et al.*, Confinement of superconducting fluctuations due to emergent electronic inhomogeneities. *Phys. Rev. B* **93**, 144509 (2016).
10. S. V. Postolova *et al.*, Superconductivity in a disordered metal with unscreened Coulomb interactions. *Phys. Rev. Research* **2**, 033307 (2020).
11. P. Giraldo-Gallo *et al.*, Field-tuned superconductor-insulator transition in $BaPb_{1-x}Bi_xO_3$. *Phys. Rev. B Condens. Matter Mater. Phys.* **85**, 174503 (2012).
12. P. Giraldo-Gallo, H. Lee, M. R. Beasley, T. H. Geballe, I. R. Fisher, Inhomogeneous superconductivity in $BaPb_{1-x}Bi_xO_3$. *J. Supercond. Nov. Magn.* **26**, 2675–2678 (2013).
13. P. Giraldo-Gallo *et al.*, Stripe-like nanoscale structural phase separation in superconducting $BaPb_{1-x}Bi_xO_3$. *Nat. Commun.* **6**, 8231 (2015).

14. D. T. Harris *et al*., Superconductivity-localization interplay and fluctuation magnetoresistance in epitaxial $BaPb_{1-x}Bi_xO3$ thin films. *Phys. Rev. Mater.* **2**, 041801 (2018).
15. Ø. Fischer, M. Kugler, I. Maggio-Aprile, C. Berthod, C. Renner, Scanning tunneling spectroscopy of high-temperature superconductors. *Rev. Mod. Phys.* **79**, 353–419 (2007).
16. S. Mizuta *et al*., STM/STS study on electronic superstructures in the superconducting state of high-T_c cuprate $Bi_2Sr_2CaCu_2O_{8+\delta}$. *J. Phys. Conf. Ser.* **969**, 012071 (2018).
17. X. L. Peng *et al*., Observation of topological transition in high-T_c superconducting monolayer $FeTe_{1-x}Se_x$ films on $SrTiO_3$(001). *Phys. Rev. B* **100**, 155134 (2019).
18. B. Sacépé *et al*., Disorder-induced inhomogeneities of the superconducting state close to the superconductor-insulator transition. *Phys. Rev. Lett.* **101**, 157006 (2008).
19. B. Sacépé *et al*., Localization of preformed Cooper pairs in disordered superconductors. *Nat. Phys.* **7**, 239–244 (2011).
20. P. Szabó *et al*., Fermionic scenario for the destruction of superconductivity in ultrathin MoC films evidenced by STM measurements. *Phys. Rev. B* **93**, 014505 (2016).
21. M. Mondal *et al*., Phase fluctuations in a strongly disordered *s*-wave NbN superconductor close to the metal-insulator transition. *Phys. Rev. Lett.* **106**, 047001 (2011).
22. M. Chand *et al*., Phase diagram of the strongly disordered *s*-wave superconductor NbN close to the metal-insulator transition. *Phys. Rev. B Condens. Matter Mater. Phys.* **85**, 014508 (2012).
23. F. C. Niestemski *et al*., A distinct bosonic mode in an electron-doped high-transition-temperature superconductor. *Nature* **450**, 1058–1061 (2007).
24. J. Zhao *et al*., Electron-spin excitation coupling in an electron-doped copper oxide superconductor. *Nat. Phys.* **7**, 719–724 (2011).
25. C. Carbillet *et al*., Spatial cross-correlations between local electron-electron interaction effects and local superconducting energy gap in moderately-disordered NbN ultrathin films. *Phys. Rev. B* **102**, 024504 (2020).
26. F. Boschini *et al*., Collapse of superconductivity in cuprates via ultrafast quenching of phase coherence. *Nat. Mater.* **17**, 416–420 (2018).
27. A. Kamlapure *et al*., Spatial variation of the two-fold anisotropic superconducting gap in a monolayer of $FeSe_{0.5}Te_{0.5}$ on a topological insulator. *Phys. Rev. B* **95**, 104509 (2017).
28. Y. Dubi, Y. Meir, Y. Avishai, Nature of the superconductor-insulator transition in disordered superconductors. *Nature* **449**, 876–880 (2007).
29. V. M. Galitski, A. I. Larkin, Disorder and quantum fluctuations in superconducting films in strong magnetic fields. *Phys. Rev. Lett.* **87**, 087001 (2001).
30. Z. Li, G. Antonius, M. Wu, F. H. da Jornada, S. G. Louie, Electron-phonon coupling from *Ab Initio* linear-response theory within the GW method: Correlation-enhanced interactions and superconductivity in $Ba_{1-x}K_xBiO_3$. *Phys. Rev. Lett.* **122**, 186402 (2019).
31. B. A. Baumert, Barium potassium bismuth oxide: A review. *J. Supercond.* **8**, 175–181 (1995).
32. S. Pei *et al*., Structural phase diagram of the $Ba_{1-x}K_xBiO_3$ system. *Phys. Rev. B Condens. Matter* **41**, 4126–4141 (1990).
33. C. H. P. Wen *et al*., Unveiling the superconducting mechanism of $Ba_{0.51}K_{0.49}BiO_3$. *Phys. Rev. Lett.* **121**, 117002 (2018).
34. M. Tinkham, *Introduction to Superconductivity. Dover Books on Physics and Chemistry* (Dover, 1996).
35. S. Bose *et al*., Competing effects of surface phonon softening and quantum size effects on the superconducting properties of nanostructured Pb. *J. Phys. Condens. Matter* **21**, 205702 (2009).
36. T. Ekino, J. Akimitsu, Superconducting energy gap in $BaPb_{1-x}Bi_xO_3$ determined from point-contact tunneling. *J. Phys. Soc. Jpn.* **58**, 2135–2139 (1989).
37. K. Luna, P. Giraldo-Gallo, T. Geballe, I. Fisher, M. Beasley, Disorder driven metal-insulator transition in $BaPb_{1-x}Bi_xO_3$ and inference of disorder-free critical temperature. *Phys. Rev. Lett.* **113**, 177004 (2014).
38. M. Suzuki, K. Komorita, M. Nagano, L. Rinderer, Tunneling studies of $BaPb_{0.75}Bi_{0.25}O_3$. *J. Phys. Soc. Jpn.* **61**, 3230–3238 (1992).
39. T. Inamura, T. Murakami, T. Inukai, Y. Enomoto, M. Suzuki, New materials for Josephson junction devices. *Jpn. J. Appl. Phys.* **21**, 313 (1982).
40. E. Climent-Pascual, N. Ni, S. Jia, Q. Huang, R. J. Cava, Polymorphism in $BaPb_{1-x}Bi_xO_3$ at the superconducting composition. *Phys. Rev. B Condens. Matter Mater. Phys.* **83**, 174512 (2011).
41. S. Ikegaya, S. Kobayashi, Y. Asano, Symmetry conditions of a nodal superconductor for generating robust flat-band Andreev bound states at its dirty surface. *Phys. Rev. B* **97**, 174501 (2018).
42. A. Ghosal, M. Randeria, N. Trivedi, Inhomogeneous pairing in highly disordered *s*-wave superconductors. *Phys. Rev. B Condens. Matter Mater. Phys.* **65**, 014501 (2001).
43. I. Roy, R. Ganguly, H. Singh, P. Raychaudhuri, Robust pseudogap across the magnetic field driven superconductor to insulator-like transition in strongly disordered NbN films. *Eur. Phys. J. B* **92**, 49 (2019).
44. M. V. Fistul, V. M. Vinokur, T. I. Baturina, Collective Cooper-pair transport in the insulating state of Josephson-junction arrays. *Phys. Rev. Lett.* **100**, 086805 (2008).
45. D. Nicoletti *et al*., Anomalous relaxation kinetics and charge-density-wave correlations in underdoped $BaPb_{1-x}Bi_xO_3$. *Proc. Natl. Acad. Sci. U.S.A.* **114**, 9020–9025 (2017).
46. S. Tajima *et al*., Optical study of the metal-semiconductor transition in $BaPb_{1-x}Bi_xO_3$. *Phys. Rev. B Condens. Matter* **32**, 6302–6311 (1985).
47. S. Tajima *et al*., Electronic states of $BaPb_{1-x}Bi_xO_3$ in the semiconducting phase investigated by optical measurements. *Phys. Rev. B Condens. Matter* **35**, 696–703 (1987).
48. A. C. Fang *et al*., Gap-inhomogeneity-induced electronic states in superconducting $Bi_2Sr_2CaCu_2O_{8+\delta}$. *Phys. Rev. Lett.* **96**, 017007 (2006).
49. A. Rogachev, B. Sacépé, Deficiency of the scaling collapse as an indicator of a superconductor-insulator quantum phase transition. *Phys. Rev. B* **101**, 235164 (2020).
50. M. C. Diamantini, C. A. Trugenberger, V. M. Vinokur, Confinement and asymptotic freedom with Cooper pairs. *Commun. Phys.* **1**, 77 (2018).
51. M. C. Diamantini, C. A. Trugenberger, V. M. Vinokur, Quantum magnetic monopole condensate. *Commun. Phys.* **4**, 25 (2021).
52. M. C. Diamantini, C. A. Trugenberger, V. M. Vinokur, Topological nature of high temperature superconductivity. *Adv. Quantum Technol.* **2021**, 2000135 (2021).
53. B. Fan, A. M. García-García, Superconductivity at the three-dimensional Anderson metal-insulator transition. *Phys. Rev. B* **102**, 184507 (2020).